

# Spinons and triplons in spatially anisotropic frustrated antiferromagnets

Masanori Kohno<sup>1,2</sup>, Oleg A. Starykh<sup>3</sup>, and Leon Balents<sup>1</sup>

<sup>1</sup>*Department of Physics, University of California, Santa Barbara, CA 93106, USA*

<sup>2</sup>*Computational Materials Science Center, National Institute for Materials Science, Tsukuba 305-0047, Japan*

<sup>3</sup>*Department of Physics, University of Utah, Salt Lake City, UT 84112, USA*

(Dated: February 1, 2008)

The search for elementary excitations with fractional quantum numbers is a central challenge in modern condensed matter physics. We explore the possibility in a realistic model for several materials, the spin-1/2 spatially anisotropic frustrated Heisenberg antiferromagnet in two dimensions. By restricting the Hilbert space to that expressed by exact eigenstates of the Heisenberg chain, we derive an effective Schrödinger equation valid in the weak interchain-coupling regime. The dynamical spin correlations from this approach agree quantitatively with inelastic neutron measurements on the triangular antiferromagnet  $\text{Cs}_2\text{CuCl}_4$ . The spectral features in such antiferromagnets can be attributed to two types of excitations: descendents of one-dimensional spinons of individual chains, and coherently propagating “triplon” bound states of spinon pairs. We argue that triplons are generic features of spatially anisotropic frustrated antiferromagnets, and arise because the bound spinon pair lowers its kinetic energy by propagating between chains.

PACS numbers:

One of the most dramatic effects of strong interactions in electronic materials is the emergence of particles with fractional quantum numbers, for example charge  $e/3$  Laughlin quasiparticles in the fractional quantum Hall effect, and spin-charge separated excitations in one dimensional (1D) quantum wires and carbon nanotubes. Indeed, fractionalization is known to be quite generic in 1D conductors and magnets.[1, 2] In this case the spin excitation carrying a fractional quantum number, spin 1/2, is referred to as a spinon [3, 4]. In contrast, in dimensions higher than one, the elementary excitation from a magnetically ordered states is known as a magnon and carries spin 1 [5, 6, 7]. Nevertheless, fractionalization caused by strong quantum fluctuations has been repeatedly identified theoretically as a possible phenomena underlying unusual experimental behavior of strongly correlated materials in two and three dimensions and zero magnetic field, such as high-temperature superconductors, heavy fermions, and frustrated quantum magnets. In these contexts, resonating valence bond (RVB) theories [8, 9] and slave-particle approaches [10, 11, 12] have been developed to describe fractionalization in dimensions greater than one[13]. However, these approaches remain largely unproved. Considerable effort has been devoted to the search for such exotic behaviors for decades [14, 15], and only recently, experimental indications of fractionalized particles [16, 17] and disordered ground states [18, 19, 20, 21] have been observed in highly frustrated antiferromagnets in two dimensions (2D).

In this paper, we consider how spinons may appear in a 2D magnet as descendents of their 1D counterparts. Our focus is the spin-1/2 spatially anisotropic antiferromagnetic Heisenberg model defined by the following Hamiltonian:

$$\mathcal{H} = \sum_{x,y} (J\mathbf{S}_{x+1,y} + J'_1\mathbf{S}_{x,y+1} + J'_2\mathbf{S}_{x+1,y+1} + J'_3\mathbf{S}_{x-1,y+1}) \cdot \mathbf{S}_{x,y}, \quad (1)$$

where  $\mathbf{S}_{x,y}$  is the spin-1/2 operator at site  $(x,y)$ . Here,  $J$  denotes the intrachain coupling, and  $J'_1$ ,  $J'_2$  and  $J'_3$  are interchain couplings as illustrated in Fig. 1. We take all the coupling constants positive, reflecting antiferromagnetic interactions, focusing on the frustrated situation  $J'_1 = J'_2 + J'_3$ . The main result of this paper is a systematic method to calculate the *inelastic* magnetic structure factor  $S(k,\omega)$  for the full range of energy transfers with  $\omega$  varying from essentially zero to large scales of several times  $J$ . The result is valid provided only  $J'_a/J$  is not too large, and indeed reveals characteristic features of spinon excitations.

One strong motivation to study this model comes from experiments on the material  $\text{Cs}_2\text{CuCl}_4$ , a spin-1/2 Heisenberg antiferromagnet on a spatially anisotropic triangular lattice. This corresponds to Eq.(1) with  $J'_1 = J'_2 \equiv J'$  and  $J'_3 = 0$ , and the *measured* anisotropy is  $J/J' \approx 3$ . [22] The spectral weight in the dynamical structure factor,  $S(k,\omega)$ , measured in this compound is dominated by a broad continuum, extending up to energy above  $3J$ , with the usually strong magnon peak appearing uncharacteristically insignificant. The spectral tail for some directions in momentum space is well-fitted by a power-law form[16, 17]. Following this observation, numerous theories have attributed the behavior to fractionalized excitations of exotic *two dimensional* critical and/or spin liquid states.[23, 24, 25] Other works have compared the data to anharmonic spin wave theory. Though the latter calculations reproduce the *shape* of the observed dispersion of the (broad) peaks in  $\text{Cs}_2\text{CuCl}_4$ , a substantial phenomenological renormalization of the exchange parameters must be included *by hand* to achieve quantitative agreement.[16, 17, 26, 27] However, numerical series expansion calculations using the un-renormalized measured  $J, J'$  values properly reproduce the experimental peak dispersion.[28, 29]

In this paper, we argue that the spectra in  $\text{Cs}_2\text{CuCl}_4$  indeed reflect the presence of spinon excitations as originally suggested, but that these spinons are descendants of the 1D excitations of the chains formed by the strong  $J$  bonds, and not characteristic of any exotic 2D state. A popular argument *against* this notion has been that the peak energy has substantial dispersion in the direction *transverse* to the chains. We show that contrary to naïve expectations, such dispersion does appear in a quasi-1D approach. The basic physics involved is the *binding* of two spinons into a delocalized and dispersing spin-1 pair (triplon). This is driven by kinetic energy, since only a pair of spinons may hop between chains. The idea is a lower dimensional analogue of Anderson’s interlayer tunneling mechanism of high temperature superconductivity, with spinon pairs replacing Cooper pairs[30, 31]. Triplon formation leads to specific signatures in the structure factor *which are indeed present in the data on  $\text{Cs}_2\text{CuCl}_4$* .

The appropriateness of the 1D approach is reinforced by several works. Ref.[32] demonstrated that it quantitatively reproduces most of the complex low temperature phase diagram observed in applied magnetic fields in  $\text{Cs}_2\text{CuCl}_4$ . It also showed that the frustrated  $J'$  coupling is ineffective in establishing long-range order: the characteristic energy scale for ordering is only of order  $(J')^4/J^3$ , much smaller than the bare  $J'$  inter-chain exchange energy. An early indication of this ineffectiveness appeared in Ref. [33], in which a “decoupled” state was suggested. More recently, the exact diagonalization study in Ref. [34] found that correlations between spins in neighboring chains remain extremely weak for  $J' \leq 0.7J$ .

This suggests that the elementary excitations (spinons) of independent spin chains are a natural basis. We therefore *project* the Hamiltonian in Eq.(1) into the subspace of eigenstates of the 1D decoupled chains [35, 36]. Each eigenstate can be characterized by the *number of excited spinons*, which is always even for any physical state. Remarkably, truncating to the first non-trivial approximation of only zero- or two-spinon states reproduces the main features of the spectrum of such quasi-one-dimensional frustrated antiferromagnets. Note that the two-spinon approximation is *not* a low-energy one (unlike the familiar and powerful “bosonization” technique) as it includes spinons with energies reaching up to  $\pi J/2 \gg J'$ . This is essential for comparison with inelastic neutron scattering data which extends over this full range.[17]

The two-spinon states of a single chain are characterized by two continuous quantum numbers, which can be thought of either as the momenta  $k_{x1}, k_{x2}$  of the individual (unbound) spinons, or equivalently, the total momentum  $k_x = k_{x1} + k_{x2}$  and (excitation) energy  $\epsilon = \epsilon_s(k_{x1}) + \epsilon_s(k_{x2})$  of the pair. We use the latter notation for convenience. The spinon energy is given by des Cloizeaux-Pearson dispersion,  $\epsilon_s(k_x) = (\pi J/2)|\sin(k_x)|$  [37]. The states can also be characterized by their total spin and  $S^z$  quantum numbers. Only the triplet ( $s = 1$ ) states are relevant to the neutron structure factor, and one may specialize without loss of generality to the  $S^z = +1$  state, which we denote  $|k_x, \epsilon\rangle_y$  on chain  $y$ . For the many-chain system, the unperturbed ground state and two-spinon basis states are given as  $|\text{G.S.}\rangle_0 \equiv \otimes_y |0\rangle_y$  and  $|k_x, \epsilon, y\rangle \equiv |k_x, \epsilon\rangle_y \otimes_{y' \neq y} |0\rangle_{y'}$ , respectively. Here,  $|0\rangle_y$  denotes the ground state of the  $y$ -th Heisenberg chain, of length  $L_x$ .

We choose to work with eigenstates of the total 2D momentum vector  $\mathbf{k} = (k_x, k_y)$ . Such  $k_y$  eigenstates are superpositions:  $|\epsilon\rangle_{\mathbf{k}} \equiv |k_x, k_y; \epsilon\rangle \equiv \frac{1}{\sqrt{L_y}} \sum_y e^{ik_y y} |k_x, \epsilon, y\rangle$  (here  $L_y$  is the number of chains). Note that, because the two spinons comprising any of the original basis states always live in the same chain, there is only one intrinsic transverse momentum  $k_y$  and not two distinct spinon momenta in the  $y$  direction. Thus there is only a one parameter ( $\epsilon$ ) set of two-spinon states for each  $k_x, k_y$ . Therefore the eigenstates in this basis take the form

$$|\Psi_{\mathbf{k}}\rangle = \int d\epsilon D_{k_x}(\epsilon) \psi_{\mathbf{k}}(\epsilon) |\epsilon\rangle_{\mathbf{k}}, \quad (2)$$

where  $D_{k_x}(\epsilon) = \Theta(\omega_{2,u}(k_x) - \epsilon) \Theta(\epsilon - \omega_{2,l}(k_x)) / \sqrt{\omega_{2,u}^2(k_x) - \epsilon^2}$  is the density of states of the Heisenberg chain, divided by  $L_x/(2\pi)$ , at momentum  $k_x$  and excitation energy  $\epsilon$  [38] ( $\Theta$  denotes the step function). It is restricted to  $\omega_{2,l}(k_x) < \epsilon < \omega_{2,u}(k_x)$ , where the boundaries of the two-spinon continuum are  $\omega_{2,l}(k) = \epsilon_s(k_x)$  and  $\omega_{2,u}(k_x) = \pi J \sin[k_x/2]$ . The wavefunction  $\psi_{\mathbf{k}}(\epsilon)$  defines the spread of the eigenstate amongst this continuum. The condition that  $|\Psi_{\mathbf{k}}\rangle$  is an eigenstate of the Hamiltonian in the 2-spinon subspace implies the Schrödinger equation:

$$\epsilon \psi_{\mathbf{k}}(\epsilon) + \int d\tilde{\epsilon} D_{k_x}(\tilde{\epsilon}) J'(\mathbf{k}) A_{k_x}^*(\epsilon) A_{k_x}(\tilde{\epsilon}) \psi_{\mathbf{k}}(\tilde{\epsilon}) = E \psi_{\mathbf{k}}(\epsilon), \quad (3)$$

where  $E$  is the excitation energy above the ground state, and  $J'(\mathbf{k}) \equiv 2(J'_1 \cos k_y + J'_2 \cos(k_x + k_y) + J'_3 \cos(k_x - k_y))$  is the Fourier transform of the interchain exchange interaction. The matrix element  $A_{k_x}(\epsilon) \equiv \frac{1}{\sqrt{2}} \langle 0 | S_{-k_x, y}^- | k_x, \epsilon \rangle_y$ , which is crucial for this study, was obtained exactly in Ref. [39] (see Supplementary Material).

We solved the integral equation, Eq.(3), numerically by carefully discretizing  $\epsilon$  to obtain a complete (in the two spinon subspace) set of eigenfunctions  $\psi_{n\mathbf{k}}$  (and corresponding states  $|\Psi_{n\mathbf{k}}\rangle$ ) and energies  $E_{n\mathbf{k}}$ , with  $n = 1 \dots M$ . Here we typically took the number of discretized energies  $M$  to be several thousand, as large as necessary to ensure good

resolution. Knowing these eigenstates, we can directly evaluate their contribution to the zero temperature dynamical structure factor  $S(\mathbf{k}, \omega)$ :

$$S(\mathbf{k}, \omega) = \int \frac{dt}{2\pi} e^{i\omega t} \langle \text{G.S.} | S_{-\mathbf{k}}^\alpha(t) S_{\mathbf{k}}^\alpha(0) | \text{G.S.} \rangle = \sum_n |\langle \text{G.S.} | S_{-\mathbf{k}}^\alpha | \Psi_{n\mathbf{k}} \rangle|^2 \delta(\omega - E_{n\mathbf{k}}). \quad (4)$$

For consistency, we approximate the ground state  $|\text{G.S.}\rangle$  by its perturbative form to first order in  $J'(\mathbf{k})$ , though the linear correction term has little effect on the results. Details are given in the Supplementary Material.

Somewhat unexpectedly, it is possible to show analytically that the structure factor obtained in this way has nearly the same form as found in the well-known random phase approximation (RPA). In particular, as shown in the Supplementary Material, when the  $O(J')$  correction to the ground state is neglected,

$$S(\mathbf{k}, \omega) = \frac{S_{1D}(k_x, \omega)}{[1 + J'(\mathbf{k})\chi'_{1D}(k_x, \omega)]^2 + [J'(\mathbf{k})\chi''_{1D}(k_x, \omega)]^2}. \quad (5)$$

Here  $S_{1D}(k_x, \omega) = \chi''_{1D}(k_x, \omega)/\pi = D_{k_x}(\omega)|A_{k_x}(\omega)|^2$  is the two-spinon structure factor of a single chain [42], and  $\chi'_{1D}(k_x, \omega) = \int_0^\infty d\omega' S_{1D}(k_x, \omega')/(\omega' - \omega)$ . This nearly coincides with the RPA expression, which is obtained by replacing our  $\chi$  with the dynamic susceptibility of a single chain,  $\chi'_{1D} \rightarrow \text{Re}\chi_{1D}$ ,  $\chi''_{1D} \rightarrow \text{Im}\chi_{1D}$ .  $\text{Re}\chi_{1D}$  differs from  $\chi'_{1D}$  by a small contribution from  $\omega' < 0$ . However, the differences between the RPA and our two-spinon result, with or without the ground state correction, are very small in all situations of interest – see Supplementary Material.

We find three types of distinctive spectral features depending on the momentum, determined by the value of  $J'(\mathbf{k})$ :

1.  $J'(\mathbf{k}) < 0$ :  $S(k, \omega)$  has a  $\delta$ -function peak below the continuous spectrum. A typical example is shown in Fig. 2 (a). As discussed above, this peak arises from a triplon bound state of two spinons,  $|\Psi_{1\mathbf{k}}\rangle$ . The triplon dispersion  $\omega_t(\mathbf{k})$  is determined from the pole of (5) where

$$1 + J'(\mathbf{k})\chi'_{1D}(k_x, \omega_t(\mathbf{k})) = 0 \quad (6)$$

and  $\chi''_{1D}(k_x, \omega_t(\mathbf{k})) = 0$  outside the continuum. The pole appears below  $\omega_{2,l}$  because there  $\chi'_{1D}$  is positive. The inter-chain dispersion of the triplon is due to the  $k_y$ -dependence of  $J'(\mathbf{k})$ . In the weak interchain-coupling regime, the spectral weight  $Z$  and binding energy  $\delta E = \omega_{2,l}(k_x) - \omega_t(\mathbf{k})$  of the peak are small, and behave as  $Z \sim |J'(k_x, k_y)|$  and  $\delta E \sim |J'(k_x, k_y)|^2$  (up to logarithmic corrections). See the Supplementary Material for details.

2.  $J'(\mathbf{k}) > 0$ : The spectral weight shifts upwards, and the peak is broadened in the continuum, see Fig. 2 (b). A suppression of spectral weight at the lower edge of the continuum occurs due to repulsion between the two spinons. When  $J'(k_x, k_y)$  is sufficiently large, a  $\delta$ -function peak appears *above* the two-spinon continuum. This peak corresponds to an anti-bound triplon state. However, the anti-bound peak is broadened by the four-spinon contribution, which leads to non-zero spectral density above the two-spinon upper-boundary,  $\omega > \omega_{2,u}$  [40].
3.  $J'(\mathbf{k}) = 0$ : For such momenta, the structure factor is *identical* in the two-spinon approximation to that of a set of decoupled chains. For the frustrated situation of principle interest, where  $J'_1 = J'_2 + J'_3$ , this condition is always satisfied for  $k_x = \pi$  (but it may also be true elsewhere).

Now, let us compare the above features with the experimental results [16, 17] on  $\text{Cs}_2\text{CuCl}_4$ . The coupling constants are experimentally estimated as  $J=0.374(5)$  meV,  $J' = J'_1=J'_2=0.128(5)$  meV, which leads to the ratio  $J'/J=0.34(3)$  [22]. This compound also has some very weak additional Dzyaloshinskii-Moriya and interplane interactions not included in our model. These have significant effects only at very low energies, e.g. in inducing long-range order in the ground state and weak incommensurability of the ordering wave vector [32, 41]. The coupling constants of these interactions are experimentally estimated as about  $0.05J$  [22]. In this paper, we neglect them for simplicity and discuss the physics for energies higher than about  $0.1J$  – note that the majority of the features in the neutron scattering data in Refs. [16, 17] are in this higher energy regime. In the notation of Refs. [16, 17], the Fourier component of the interchain couplings reads  $J'(\mathbf{k}) = 4J' \cos(k'_x/2) \cos(k'_y/2)$ , where  $k'_x$  and  $k'_y$  are the momenta corresponding to  $b$  and  $c$  axes in Refs. [16, 17], respectively:  $k'_x = k_x$  and  $k'_y = k_x + 2k_y$ .

First, we discuss the large tail of  $S(\mathbf{k}, \omega)$  and the interpretation of the power-law behaviors observed in  $\text{Cs}_2\text{CuCl}_4$  [17]. In the present approach, a power-law behavior at the lower edge of the continuum ( $\omega_{2,l}$ ) is obtained only when  $J'(\mathbf{k}) = 0$ . There, we expect the same behavior as occurs in decoupled Heisenberg chains, i.e.  $S(\mathbf{k}, \omega) \propto \sqrt{-\ln[\omega - \omega_{2,l}]/[\omega - \omega_{2,l}]}$  at  $k_x \neq \pi$ , and  $S(\mathbf{k}, \omega) \propto \sqrt{-\ln\omega/\omega}$  at  $k_x = \pi$  near the lower edge of continuum [42]. On a spatially anisotropic triangular lattice,  $J'(\mathbf{k})$  is zero on the lines of  $k_x = \pi$  and  $k_y = (\pi - k_x)/2$  in momentum space, which correspond to the lines of  $k'_x = \pi$  and  $k'_y = \pi$ . The experimental result at  $k'_x = \pi$  is given as the G scan in Ref.

[17]. The comparison of  $S(\mathbf{k}, \omega)$  at  $k'_x = \pi$  between the present result (i.e.  $S_{1D}(k, \omega)$  of the Heisenberg chain) and the experimental data (G scan in Fig. 5 of Ref. [17]) is shown in Fig. 3. Only a single fitting parameter – for the global height of intensity in this plot – has been employed. For all further comparisons (below), we will employ the same normalization, so the remaining comparisons are parameter-free. Although the theoretical curve and experimental data differ somewhat at low energies due to the neglect of long-range magnetic order and the Dzyaloshinskii-Moriya interaction in the theory, the agreement at higher energy is quite good.

We next turn to the dispersion relation, which we define here, in order to ease comparison with experimental data, by the location of the peak  $\omega(\mathbf{k})$  in  $S(\mathbf{k}, \omega)$  at each  $\mathbf{k}$ . A comparison of our result and the experimental data (from Fig. 3 in Ref. [17]) is shown in Fig. 4. It should be noted that there is no fitting parameter in this plot. The asymmetry of the dispersion relation of the main peak with respect to  $k'_x = \pi$  and  $3\pi$  observed at  $k'_y = 0$  and  $2\pi$  is consistently reproduced by the present approach (Fig. 4 (a,b)). At  $k'_y = 3\pi$ , the dispersion relation is symmetric because  $J'(\mathbf{k})$  is zero at this momentum, which is also consistent with the experimental observation (Fig. 4 (c)). Despite the 1D starting point of the approach, it explains the experimental dependence upon transverse momentum ( $k'_y$ ) as well. Figure 4 (d,e) shows  $S(\mathbf{k}, \omega)$  in the perpendicular direction to  $k'_x$  at  $k'_x = -\pi/2$ . The sign of  $J'(\mathbf{k})$  changes at  $k'_y = 3\pi$ . This causes the following change in  $S(\mathbf{k}, \omega)$ : As shown in Fig. 4 (e), a bound state is formed just below the continuum for  $k'_y < 3\pi$ . On the other hand, for  $k'_y > 3\pi$ , the spectral weight shifts upwards, and the peak is broadened and absorbed into the continuum. Put simply, *the lower edge of continuum (open squares in Fig. 4 (a- d)) lies below the peak only in the region of  $J'(\mathbf{k}) > 0$ , and the main peak is always observed at the lowest energy of the spectrum for  $J'(\mathbf{k}) \leq 0$* . These features are exactly in accord with the theoretical predictions. Moreover, for  $J'(\mathbf{k}) < 0$ , the peak is much sharper (in fact resolution limited) than for  $J'(\mathbf{k}) > 0$ . This is illustrated in Figs. 4 (f,g), which compare our theoretical predictions to scans E,F of Ref. 17 – note the factor of 4 larger scale in Fig. 4 (f) compared to Fig. 4 (g).

Furthermore, the asymmetry of the experimental estimate of the upper edge of continuum with respect to  $k'_x = \pi$  or  $k'_y = 3\pi$  is also qualitatively understood: At the momenta with  $J'(\mathbf{k}) > 0$ , the spectral weight shifts upwards, and the high-energy weight becomes larger. On the other hand, in the region of  $J'(\mathbf{k}) < 0$ , the high-energy weight decreases, because part of it shifts into the bound state (Figs. 2 and 4 (e)). This feature is consistent with the behavior of the upper edge of continuum observed in the experiment (open circles in Fig. 4 (a-d)). Namely, the peak of the dispersion relation of the upper edge of continuum is observed at the momentum a little shifted toward the region of  $J'(\mathbf{k}) > 0$  from  $k'_x = \pi$  or  $k'_y = 3\pi$ .

Our approach allows for systematic improvements by including further multi-spinon states. As a first step, we included the four-spinon states in the RPA approximation. This is done numerically by expressing the matrix element in Eq.(4) for a finite length Heisenberg chain as a product of determinants[43, 44, 45]. The sum rule for the total spectral weight and the first frequency moment is satisfied by more than 99% for the length ( $L_x = 288$ ) considered. We then calculate from this Eq.(5) using  $\chi'_{1D} \rightarrow \text{Re}\chi_{1D}$  and  $\chi''_{1D} \rightarrow \text{Im}\chi_{1D}$  and obtain the two-dimensional  $S(\mathbf{k}, \omega)$ . We note that the finite-size errors for  $L_x = 288$  are insignificant compared to the instrumental resolution. The resulting changes are small but very encouraging – the bound state in scan E has moved down a little, making agreement with experimental data essentially perfect (see Fig. 4 (f)). We also observe that the anti-bound states, being located in the region of  $\omega - \mathbf{k}$  space with non-zero spectral weight for 4-spinon excitations, acquire a non-zero linewidth as expected, but that this is small enough that they remain visible features.

We conclude with a general discussion of our method and its ramifications. The most significant feature is the emergence of a spinon bound state driven by kinetic energy. Despite the superficial similarity to the more familiar *magnon*, the physics of the bound state is quite distinct. Specifically, a magnon is a Goldstone mode which emerges in a long-range ordered magnet as a consequence of broken symmetry. In our calculations, no such broken symmetry is presumed. Instead, the bound state is a true  $s = 1$  triplet excitation, and is better characterized as a *triplon* than a magnon. The same is true for the anti-bound state. In fact, the anti-bound triplon is directly analogous to the *zero sound* mode of a neutral interacting Fermi gas[46].

Since in most cases, weakly coupled spin chains *do* eventually order at low enough temperature, it is important to understand the validity of our scheme in this situation. For this, it is crucial that we consider *frustrated* inter-chain couplings ( $J'_1 = J'_2 + J'_3$ ). In this case, the leading divergence associated with coupling neighboring chains – the strong tendency to Néel order at  $k_x = \pi$  within each chain – is removed because  $J'(\pi, k_y) = 0$ . Without this condition, one obtains[47, 48] strong long-range Néel order which influences spectral features on the scale of  $O(J')$ . Since this effect is comparable to those captured by the two-spinon approximation, the latter is unjustified without frustration. With frustration, any fluctuation-induced order has a much smaller characteristic energy scale[32, 41, 49], and can be neglected compared to the shifts of excited states captured by the present approach. Of course, the presence of *any* long-range order, however weak, does modify some excitations in a qualitative manner. The triplon, when present, is expected to transform smoothly into a magnon as a consequence. In regions of momentum space where no bound state is present below the continuum,  $J'(\mathbf{k}) > 0$ , a magnon may weakly emerge as a consequence of long-range order.

There are numerous important directions for extensions and applications. It would be interesting to compare with neutron measurements of  $\text{Cs}_2\text{CuBr}_4$ , which is isostructural and can be modeled similarly to  $\text{Cs}_2\text{CuCl}_4$  but

with somewhat larger  $J'/J \approx 0.5$ [50], and to search for signs of the anti-bound triplon in either material. Some theoretical extensions would be to include three-dimensional and Dyzalooshinskii-Moriya couplings, systematically treat higher-spinon states, to include thermal fluctuations at  $T > 0$ , and to take into account weak long-range order. A very interesting different direction is to apply analogous methods to spatially anisotropic strongly interacting *conductors*, modeled by Hubbard or  $t$ - $J$  type Hamiltonians. Given the very small arsenal of theoretical techniques capable of reliably obtaining intermediate energy spectra in strongly interacting systems above one dimension, further investigation of such methodology seems highly worthwhile. We would like to thank J. Alicea, M.P.A. Fisher and R. Shindou for discussions. This work is supported by the Grant-in-aid for Scientific Research (C) No. 10354143 from MEXT, Japan (M. K.), the Petroleum Research Fund ACS PRF 43219-AC10 (O. S.), NSF grant/DMR-0457440 (L. B.) and the Packard Foundation (L. B.). Part of this research was completed at KITP and supported in part by NSF under Grant No. PHY05-51164.

## Supplementary Material

### Basis

The two-spinon states of a single chain are characterized by two continuous quantum numbers, which can be thought of either as the momenta  $k_{x1}, k_{x2}$  of the individual (unbound) spinons, or equivalently, the total momentum  $k_x = k_{x1} + k_{x2}$  and (excitation) energy  $\epsilon = \epsilon_s(k_{x1}) + \epsilon_s(k_{x2})$  of the pair. The spinon excitation energy is given by the des Cloizeaux-Pearson dispersion relation  $\epsilon_s(k) = (\pi J/2) \sin[k]$  [37], which is seen to describe the lower boundary of the two-spinon continuum,  $\epsilon_s(k) = \omega_{2,l}(k)$ . The excitation energy of the spinon pair is then expressed via the total,  $k_x$ , and relative,  $q_x = (k_{x1} - k_{x2})/2$ , momenta of the pair  $\epsilon(k_x, q_x) = \pi J \sin[k_x/2] \cos[q_x]$ . Observe that the upper (lower) boundaries of the two-spinon continuum correspond to  $q_x = 0$  ( $\pm k_x/2$ ). We find it convenient to describe the two-spinon state of a chain in terms of the total momentum  $k_x$  and excitation energy  $\epsilon$  of the pair. The transformation from  $q_x$  to  $\epsilon$  explains the density of states factor  $D_{k_x}(\epsilon)$  appearing in (2).

To derive (3), we evaluate the expectation value of the Hamiltonian (1) in the state (2)

$$\langle \Psi | \mathcal{H} | \Psi \rangle_{\mathbf{k}} = E_0 L_x L_y + \int d\epsilon D_{k_x}(\epsilon) \epsilon |\psi_{k_x}(\epsilon)|^2 + J'(\mathbf{k}) \int d\epsilon d\tilde{\epsilon} D_{k_x}(\epsilon) D_{k_x}(\tilde{\epsilon}) A_{k_x}^*(\epsilon) A_{k_x}(\tilde{\epsilon}) \psi_{k_x}^*(\epsilon) \psi_{k_x}(\tilde{\epsilon}), \quad (7)$$

where  $E_0 = J(-\ln 2 + 1/4)$  is the ground state energy per site of decoupled chains [35, 36], and we made use of the normalization condition  $\int d\epsilon D_{k_x}(\epsilon) |\psi_{k_x}(\epsilon)|^2 = 1$  as appropriate for the state (2). “Factoring out”  $\epsilon$ -integration  $\int d\epsilon D_{k_x}(\epsilon) \psi_{k_x}^*(\epsilon)$  in (7) leads to Eq.(3) of the main text.

The ground state to two spinon matrix element  $A_{k_x}(\epsilon)$  represents the key technical element of our calculation

$$A_{k_x}(\epsilon) \equiv \sqrt{2} \langle 0 | S_{-k_x, y}^x | k_x, \epsilon \rangle_y = -i \sqrt{2} \langle 0 | S_{-k_x, y}^y | k_x, \epsilon \rangle_y. \quad (8)$$

Its absolute value squared,  $M(k_x, \epsilon) = |A_{k_x}(\epsilon)|^2$ , also called the singlet-to-triplet transition rate, is obtained exactly by an algebraic analysis based on infinite-dimensional quantum group symmetries in Ref. [39] and subsequently simplified in Ref. [42], which we follow here. The matrix element  $A$  in (8) is obtained as a square-root of  $M$  because two-spinon states with different  $k_x$  and/or  $\epsilon$  are orthogonal and thus the phase can be set to zero for every set  $(k_x, \epsilon)$  independently. Note that our choice of  $|k_x, \epsilon_{k_x/y}\rangle$  as an  $S^z = +1$  eigenstate of 2 spinons in  $y$ -th chain ensures that  $\langle 0 | S_{-k_x, y}^z | k_x, \epsilon \rangle_y = 0$ .

Specifically,  $A_k(\epsilon) = \exp[-I(t)/2]/\sqrt{4\pi}$ , where [42]

$$I(t) = -I_0 - \ln |t \sinh(\pi t/4)| + s(t), \quad s(t) = \int_0^\infty dx \frac{\sin^2[xt/2]}{x \cosh^2[x]}, \quad (9)$$

$I_0 = 0.3677\dots$  and  $k, \epsilon$  dependence comes via the parameter  $t$

$$\cosh\left[\frac{\pi t}{4}\right] = \sqrt{\frac{\omega_{2,u}^2(k) - \omega_{2,l}^2(k)}{\epsilon^2 - \omega_{2,l}^2(k)}}. \quad (10)$$

Integration of  $s(t)$  has been performed numerically by an adaptive quadrature algorithm.

### Discretization in the $\epsilon$ space

For numerical calculations, we carefully discretize energy  $\epsilon$  for every  $k_x$  value, by dividing the interval  $\omega_{2,u}(k_x) - \omega_{2,l}(k_x)$  into  $M$  discrete points. The resulting discrete  $M \times M$  eigenvalue problem is then solved for every value of momentum  $\mathbf{k} = (k_x, k_y)$ . The data points in the  $\epsilon$ -space are chosen so that the distribution of them reduces to the exact density of states of the Heisenberg chain [38] in the continuous limit:

$$\Delta\epsilon D_{k_x}(\epsilon) = \frac{|k_x|}{2M}. \quad (11)$$

Next, it is convenient to define rescaled two-spinon states with Kronecker delta function overlaps in place of the Dirac delta-function overlapping continuum states. Specifically:

$$|\epsilon\rangle^M \equiv \sqrt{\frac{|k_x|}{2M}} |\epsilon\rangle. \quad (12)$$

One can check that

$${}^M\langle\epsilon'|\epsilon\rangle^M = \frac{k_x}{2M} \langle\epsilon'|\epsilon\rangle = \frac{k_x}{2M} \frac{1}{D(\epsilon)} \delta(\epsilon - \epsilon') = \frac{k_x}{2M} \frac{1}{D(\epsilon)\Delta\epsilon} \delta_{\epsilon,\epsilon'} = \delta_{\epsilon,\epsilon'} \quad (13)$$

as desired. We also rescale wavefunction as  $\phi(\epsilon) = \sqrt{|k_x|/(2M)} \psi_{\mathbf{k}}(\epsilon)$ , suppressing for brevity its dependence on the center-of-mass momentum  $\mathbf{k}$  (it enters the problem only as a parameter). With these definitions, equation (2) takes on simple form

$$|\Psi_{\mathbf{k}}\rangle = \sum_{\epsilon} \phi(\epsilon) |\epsilon\rangle^M. \quad (14)$$

The Schrödinger equation, in turn, takes on matrix form

$$\epsilon\phi(\epsilon) + J'(\mathbf{k}) \frac{|k_x|}{2M} \sum_{\tilde{\epsilon}} A^*(\tilde{\epsilon}) A(\epsilon) \phi(\tilde{\epsilon}) = E_{\mathbf{k}} \phi(\epsilon). \quad (15)$$

We typically took the number of discretized energies  $M$  to be several thousand, as large as necessary to ensure good resolution and convergence of the results.

### Dynamical structure factor $S(k, \omega)$

The dynamical structure factor  $S(\mathbf{k}, \omega)$  is defined by

$$S(\mathbf{k}, \omega) \equiv \int \frac{dt}{2\pi} e^{i\omega t} \langle \text{G.S.} | S_{-\mathbf{k}}^{\alpha}(t) S_{\mathbf{k}}^{\alpha}(0) | \text{G.S.} \rangle, \quad (16)$$

where *no sum* on  $\alpha = x, y$  or  $z$  is implied. This is calculated within the 2-spinon subspace using the obtained eigenstates and energies of the effective Hamiltonian as

$$S(\mathbf{k}, \omega) = \frac{1}{2} \sum_{E_{\mathbf{k}}} |\langle \text{G.S.} | S_{-\mathbf{k}}^- | \Psi_{\mathbf{k}} \rangle|^2 \delta(\omega - E_{\mathbf{k}}), \quad (17)$$

where summation is over excited states of the system with momentum  $\mathbf{k}$  and energy  $\omega = E_{\mathbf{k}}$ . In Eq.(17), it is clear that, since the ground state is a singlet, only triplet excited states  $|\Psi_{\mathbf{k}}\rangle$  with total  $S^z = +1$  can contribute to the sum.

Note that

$$|\Psi_{\mathbf{k}}\rangle = \sum_{\epsilon} \frac{1}{\sqrt{L_y}} \sum_y \phi(\epsilon) e^{ik_y y} |k_x, \epsilon, y\rangle^M, \quad (18)$$

and writing  $S_{-\mathbf{k}}^- = \frac{1}{\sqrt{L_y}} \sum_{y'} e^{-ik_y y'} S_{-k_x, y'}^-$ , we have

$$S_{-\mathbf{k}}^- |\Psi_{\mathbf{k}}\rangle = \sum_{\epsilon} \frac{1}{L_y} \sum_{y, y'} \phi(\epsilon) e^{ik_y (y - y')} S_{-k_x, y'}^- |k_x, \epsilon, y\rangle^M. \quad (19)$$

This can be separated into terms with  $y' = y$  and  $y' \neq y$ . Projecting the resulting state into the subspace containing only zero or two spinons per chain, one then obtains

$$S_{-\mathbf{k}}^- |\Psi_{\mathbf{k}}\rangle = |\Upsilon\rangle_0 + |\Upsilon\rangle_1, \quad (20)$$

with components containing zero or four total spinon excitations:

$$|\Upsilon\rangle_0 = \sqrt{2} \sqrt{\frac{|k_x|}{2M}} \sum_{\epsilon} \phi(\epsilon) A_{k_x}(\epsilon) |\text{G.S.}\rangle_0, \quad (21)$$

$$|\Upsilon\rangle_1 = \sum_{\epsilon, \epsilon'} \sqrt{2} \sqrt{\frac{|k_x|}{2M}} \frac{1}{L_y} \sum_{y \neq y'} e^{ik_y(y-y')} \phi(\epsilon) A_{-k_x}^*(\epsilon') |k_x, \epsilon; S^z = +1\rangle_y^M | -k_x, \epsilon'; S^z = -1\rangle_{y'}^M \otimes_{y'' \neq y, y'} |0\rangle_{y''}. \quad (22)$$

Note that in Eq.(22) we have indicated explicitly the total  $S^z$  of the spinon pair on chains  $y, y'$ , since the two chains have equal and opposite  $S^z = \pm 1$ .

We approximate the ground state by its form to first order in  $J'(\mathbf{k})$ , in the subspace of states with zero or two spinons per chain:

$$|\text{G.S.}\rangle \approx |\text{G.S.}\rangle_0 + |\text{G.S.}\rangle_1, \quad (23)$$

with as usual, in first order perturbation theory,

$$|\text{G.S.}\rangle_1 = \frac{1}{E_0 - \mathcal{H}_0} \mathcal{H}' |\text{G.S.}\rangle_0. \quad (24)$$

Here  $\mathcal{H}_0 = \mathcal{H}|_{J'_a \rightarrow 0}$  is the decoupled chain Hamiltonian, and  $\mathcal{H}' = \mathcal{H} - \mathcal{H}_0$  contains the interchain exchange couplings.

The desired matrix element then has two terms:

$$\langle \text{G.S.} | S_{-\mathbf{k}}^- | \Psi_{\mathbf{k}} \rangle = {}_0 \langle \text{G.S.} | \Upsilon \rangle_0 + {}_1 \langle \text{G.S.} | \Upsilon \rangle_1. \quad (25)$$

The first term is simplest. From Eq.(21), one directly obtains

$${}_0 \langle \text{G.S.} | \Upsilon \rangle_0 = \sqrt{2} \sqrt{\frac{|k_x|}{2M}} \sum_{\epsilon} \phi(\epsilon) A_{k_x}(\epsilon). \quad (26)$$

Now consider the second term. To evaluate this explicitly, it is useful to write

$$\mathcal{H}' = \sum_{k_x, y} J'(k_x) \left[ \frac{1}{2} \left( S_{k_x, y}^+ S_{-k_x, y+1}^- + S_{k_x, y}^- S_{-k_x, y+1}^+ \right) + S_{k_x, y}^z S_{-k_x, y+1}^z \right]. \quad (27)$$

Because  $|\Upsilon\rangle_1$  contains only spin  $S^z = \pm 1$  spinon pairs on two chains, we can restrict the consideration of  $|\text{G.S.}\rangle_1$  to those components with the same structure. This means that the third term inside the square brackets in Eq.(27) can be neglected, since it creates  $S^z = 0$  two-spinon states on the chains  $y, y+1$ . Taking only the first two terms, we have

$$|\text{G.S.}\rangle_1 = - \sum_{k_x, y} \frac{|k_x|}{2M} J'(k_x) \sum_{\epsilon, \epsilon'} \frac{A_{k_x}^*(\epsilon) A_{-k_x}^*(\epsilon')}{\epsilon + \epsilon'} \sum_{\delta=\pm 1} |k_x, \epsilon; S^z = \delta\rangle_y^M | -k_x, \epsilon'; S^z = -\delta\rangle_{y+1}^M \otimes_{y'' \neq y, y+1} |0\rangle_{y''}. \quad (28)$$

We can then evaluate the overlap. One obtains

$${}_1 \langle \text{G.S.} | \Upsilon \rangle_1 = -\sqrt{2} \left( \frac{|k_x|}{2M} \right)^{3/2} J'(\mathbf{k}) \sum_{\epsilon, \epsilon'} \frac{\phi(\epsilon) A_{k_x}(\epsilon) A_{-k_x}^*(\epsilon') A_{-k_x}(\epsilon')}{\epsilon + \epsilon'}. \quad (29)$$

Observe that the correction diverges at  $k_x = \pi$ , where the spinons have zero energy, *unless*  $J'(k_x = \pi) = 0$ . This hints at the instability of the system towards magnetic ordering in the case of *non-frustrated* inter-chain coupling.

Combining Eqs.(29,26), the perturbation-theory- improved transition rate can be expressed as

$$|\langle \text{G.S.} | S_{-\mathbf{k}}^- | \Psi_{\mathbf{k}} \rangle|^2 = \frac{|k_x|}{M} \left| \sum_{\epsilon} \phi(\epsilon) A_{k_x}(\epsilon) \left\{ 1 - J'(\mathbf{k}) \sum_{\epsilon'} \frac{|k_x|}{2M} \frac{|A_{k_x}(\epsilon')|^2}{\epsilon + \epsilon'} \right\} \right|^2. \quad (30)$$

This and equation (17) provides way to numerically evaluate the structure factor. Fig. 5 shows that effect of the perturbative correction  ${}_1 \langle \text{G.S.} | \Upsilon \rangle_1$  on the calculated structure factor is very small.

### Connection to random-phase approximation (RPA)

It is possible to obtain an analytic solution to the integral equation describing the two-spinon states, Eq.(3). To do so, it is convenient to use the same discretization scheme as described above in Eq.(11) to resolve the wavefunctions of individual states in the continuum. The Schrödinger equation (15) is re-written as

$$\epsilon\phi(\epsilon) + B(E)A(\epsilon) = E\phi(\epsilon). \quad (31)$$

Note that the quantity

$$B(E) = \frac{J'(\mathbf{k})|k_x|}{2M} \sum_{\tilde{\epsilon}} \phi(\tilde{\epsilon})A^*(\tilde{\epsilon}) \quad (32)$$

is *independent* of  $\epsilon$ . This allows one to completely determine the  $\epsilon$  dependence of  $\phi(\epsilon)$  as

$$\phi_E(\epsilon) = \frac{B(E)A(\epsilon)}{E - \epsilon}. \quad (33)$$

Inserting this form into Eq.(32), one obtains the eigenvalue condition

$$\frac{J'(\mathbf{k})|k_x|}{2M} \sum_{\epsilon} \frac{|A(\epsilon)|^2}{E - \epsilon} = 1. \quad (34)$$

This equation has two classes of solutions. There are bound (or anti-bound) states, in which the eigenvalue  $E$  is well-separated from the continuum of the decoupled chains. Then the denominator in Eq.(34) remains finite as one takes the discretization to zero, i.e.  $M \rightarrow \infty$ . One thereby obtains the bound state condition

$$J'(\mathbf{k}) \int d\epsilon D(\epsilon) \frac{|A(\epsilon)|^2}{E - \epsilon} = 1. \quad (35)$$

The second class of solution is more subtle, and occurs when  $E$  is in the range of the continuum, i.e. for finite but large  $M$ , it is close to one of the discretized two-spinon eigenvalues of the decoupled chains, which we denote  $\epsilon_0$ . We assume (and confirm self-consistently) that the energy of such a state can be written as  $E = \epsilon_0 + \delta/M$ , where  $\delta$  remains  $O(1)$  as  $M \rightarrow \infty$ . We then rewrite Eq.(34) as

$$\frac{J'(\mathbf{k})|k_x|}{2M} \sum_{\epsilon} |A(\epsilon)|^2 \left[ \frac{\epsilon_0 - \epsilon}{(\epsilon_0 - \epsilon)^2 - (\delta/M)^2} - \frac{\delta/M}{(\epsilon_0 - \epsilon)^2 - (\delta/M)^2} \right] = 1. \quad (36)$$

The first term contains  $\epsilon_0 - \epsilon$  in the *numerator*, and the summand is locally *odd* about  $\epsilon = \epsilon_0$ . The contribution from the sum in the region where  $|\epsilon - \epsilon_0|$  is  $O(1/M)$  is therefore negligible, because the contributions from eigenvalues  $\epsilon$  on either side of  $\epsilon_0$  cancel. Conversely, there is a non-vanishing contribution from  $|\epsilon - \epsilon_0|$  of  $O(1)$ , which in the  $M \rightarrow \infty$  limit becomes a principle part integral. Conversely, in the second sum, there is only a  $\delta/M$  factor in the numerator, and the integrand is locally *even* about  $\epsilon = \epsilon_0$ . In this sum, there is an  $O(1)$  contribution from the region  $|\epsilon - \epsilon_0|$  of  $O(1/M)$ . This must be calculated explicitly, by summing over discrete  $\epsilon_n = \epsilon_0 + \Delta\epsilon n$ , with integer  $n$ . Here the level spacing is determined from  $D(\epsilon_0)\Delta\epsilon = |k_x|/(2M)$ , and because the sum is sharply peaked we can approximate  $A(\epsilon) \approx A(\epsilon_0)$ . Because the integrand decays as  $|\epsilon - \epsilon_0|^{-2}$ , the contribution from  $|\epsilon - \epsilon_0|$  of  $O(1)$  is negligible in the sum, and the limits on  $n$  can be extended to  $\pm\infty$ .

Carrying out this sum (using  $2b^2 \sum_1^\infty 1/(n^2 - b^2) = 1 - \pi b \cot(\pi b)$ ) and taking the  $M \rightarrow \infty$  limit, we find the simple result

$$\pi J'(\mathbf{k})D(\epsilon_0)|A(\epsilon_0)|^2 \cot(\pi\gamma) + J'(\mathbf{k})P \int d\epsilon \frac{D(\epsilon)|A(\epsilon)|^2}{\epsilon_0 - \epsilon} = 1, \quad (37)$$

where we have defined for convenience

$$\gamma = \frac{2D(\epsilon_0)\delta}{|k_x|} = \frac{\delta E}{\Delta\epsilon}. \quad (38)$$

This form guarantees  $|\gamma| < 1/2$ , so that the shift of the energy level  $\delta E$  is always less than half the distance to the nearest eigenvalue, i.e. the levels do not cross upon increasing  $J'$ .



Now we turn to the determination of the structure factor. Normalization of state (14) fixes  $|B(E)|$  according to

$$|B(E)|^2 = \left[ \sum_{\epsilon} \frac{|A(\epsilon)|^2}{(E - \epsilon)^2} \right]^{-1}. \quad (39)$$

This observation leads us to the structure factor, which we divide into the bound state and continuum contributions:

$$S(\mathbf{k}, \omega) = S_{\text{bs}}(\mathbf{k}, \omega) + S_{\text{cont}}(\mathbf{k}, \omega). \quad (40)$$

First consider the bound (anti-bound) state contribution – we will consider only a single bound (anti-bound) state, since this occurs for the triangular lattice of present interest. In any case, multiple states would simply give additive contributions. This gives directly a delta-function peak in the structure factor, at  $\omega = E_{bs}$ , where  $E_{bs}$  is the bound state energy:

$$S_{\text{bs}}(\mathbf{k}, \omega) = |B(E)|^2 \frac{|k_x|}{2M} \sum_{\epsilon, \epsilon'} \frac{|A(\epsilon)|^2 |A(\epsilon')|^2}{(E - \epsilon)(E - \epsilon')} \delta(\omega - E). \quad (41)$$

Using Eq.(34), this immediately simplifies to

$$S_{\text{bs}}(\mathbf{k}, \omega) = |B(E)|^2 \frac{2M}{|k_x|} \frac{1}{[J'(\mathbf{k})]^2} \delta(\omega - E). \quad (42)$$

In this case, since  $E - \epsilon$  remains non-zero as  $M \rightarrow \infty$ , the sum in Eq.(39) can be converted to an integral:

$$|B(E)|^2 = \frac{|k_x|}{2M} \left[ \int d\epsilon D(\epsilon) \frac{|A(\epsilon)|^2}{(E - \epsilon)^2} \right]^{-1}. \quad (43)$$

Thus we obtain the bound state delta-function contribution

$$S_{\text{bs}}(\mathbf{k}, \omega) = \left\{ [J'(\mathbf{k})]^2 \int d\epsilon D(\epsilon) \frac{|A(\epsilon)|^2}{(E_{bs} - \epsilon)^2} \right\}^{-1} \delta(\omega - E_{bs}). \quad (44)$$

We now turn to the continuum contribution. Following the same steps as above, we find the analog of Eq.(42),

$$S_{\text{cont}}(\mathbf{k}, \omega) = \sum_{E \neq E_{bs}} |B(E)|^2 \frac{2M}{|k_x|} \frac{1}{[J'(\mathbf{k})]^2} \delta(\omega - E). \quad (45)$$

In this case, more care must be taken in evaluating  $B(E)$  from Eq.(39), because the energy denominators in the sum become small as  $M \rightarrow \infty$ . Indeed, the sum is dominated by  $|E - \epsilon|$  of  $O(1/M)$ , and so one may as in Eq.(37) consider the density of states (i.e. spacing  $\Delta\epsilon$ ) and  $A(\epsilon)$  to be approximately constant in this region. This allows one to carry out the sum explicitly (using  $\sum_{-\infty}^{\infty} 1/(n+a)^2 = \pi^2/\sin^2(\pi a)$ ) and obtain

$$|B(E)|^2 = \frac{(\Delta\epsilon)^2}{\pi^2 \csc^2(\pi\gamma)} \frac{1}{|A(E)|^2}. \quad (46)$$

Inserting this into Eq.(45), in the large  $M$  limit the sum may be converted to an integral via  $\sum_{E \neq E_{bs}} \Delta E \rightarrow \int dE$ , and thereby collapse the delta-function. One then obtains

$$S_{\text{cont}}(\mathbf{k}, \omega) = \frac{1}{\pi^2 \csc^2(\pi\gamma)} \frac{1}{D(\omega) |A(\omega)|^2} \frac{1}{[J'(\mathbf{k})]^2}. \quad (47)$$

Using  $\csc^2(\pi\gamma) = \cot^2(\pi\gamma) + 1$  and Eq.(37), we finally arrive at

$$S_{\text{cont}}(\mathbf{k}, \omega) = \frac{S_{1D}(k_x, \omega)}{[1 + J'(\mathbf{k})\chi'(k_x, \omega)]^2 + [J'(\mathbf{k})\chi''(k_x, \omega)]^2} \quad (48)$$

with

$$\chi'(k_x, \omega) = P \int_0^\infty d\omega' \frac{D(\omega') |A(\omega')|^2}{\omega' - \omega} \text{ and } \frac{1}{\pi} \chi''(k_x, \omega) = S_{1D}(k_x, \omega) = D(\omega) |A(\omega)|^2. \quad (49)$$

The standard RPA result has the same functional form as (48) but with  $\chi', \chi''$  replaced by  $\text{Re}\chi_{\text{rpa}}, \text{Im}\chi_{\text{rpa}}$  via

$$\text{Re}\chi_{\text{rpa}}(k_x, \omega) = \frac{1}{\pi} P \int_{-\infty}^\infty d\omega' \frac{\text{Im}\chi_{\text{rpa}}(k_x, \omega')}{\omega' - \omega} \text{ and } \frac{1}{\pi} \text{Im}\chi_{\text{rpa}}(k_x, \omega) = \text{sgn}(\omega) S_{1D}(k_x, |\omega|). \quad (50)$$

The close similarity of expressions (49) and (50) is illustrated in Fig.5.

### Triplon dispersion in anisotropic triangular lattice

Bound (and antibound) states outside the continuum are determined by the condition  $1 + J'(\mathbf{k})\chi'(k_x, \omega_t(\mathbf{k})) = 0$ , which is just (35), where  $J'(\mathbf{k}) = 4J' \cos[k_x/2] \cos[k_y/2]$  for  $\text{Cs}_2\text{CuCl}_4$ .

*Bound state:* Since  $\chi' > 0$  for  $\omega < \omega_{2,l}$  as follows from (49), one needs  $J'(k_x, k_y) < 0$  for it to appear. Using the asymptotic behavior of the chain structure factor near the lower edge of the two-spinon continuum,  $\omega_{2,l}$  [42]  $S_{1D} \approx C \sqrt{-\ln[\omega - \omega_{2,l}]/[\omega_{2,l}(\omega - \omega_{2,l})]}$ , we find with logarithmic accuracy

$$\chi'(k_x, \omega \rightarrow \omega_{2,l}) = \sqrt{8C} \frac{\sqrt{-\ln[\omega_{2,l} - \omega]}}{\sqrt{\omega_{2,l}[\omega_{2,l} - \omega]}} \arctan \sqrt{\frac{\omega_{2,u} - \omega_{2,l}}{\omega_{2,l} - \omega}}. \quad (51)$$

Here  $C = \exp[I_0/2]/\sqrt{16\pi^3}$ . Provided that  $J'(\mathbf{k})$  is negative, we readily see that the triplon binding energy behaves as  $\delta E = \omega_{2,l} - \omega_t(\mathbf{k}) \propto [J'(\mathbf{k})]^2$ , up to very weak logarithmic corrections. The triplon appears below the continuum and propagates along both the  $x$  and  $y$  directions, as shown in Fig.2a.

To compare with the bound state data from the effective Schrödinger equation (3), we calculate  $S_{1D}$  and  $\chi'$  numerically. Results for the binding energy  $\delta E = \omega_{2,l} - \omega_t$  obtained in these two calculations are found to essentially coincide with each other as shown in Fig. 6. We also observe that in the regions where the width of the 2-spinon continuum becomes comparable to  $\delta E$ , the scaling changes to  $\delta E \sim J'(\mathbf{k})$ . The change from quadratic to linear scaling can be understood simply from (51), and simply corresponds to the situations where the argument of the cotangent is large (quadratic) or  $O(1)$  (linear). We also analyze spectral weight (residue)  $Z$  of the triplon, see (44). We find that for small  $J'$  it scales as  $\sqrt{\delta E} \propto J'$ . A comparison between the numerical and analytical results in a wider range of inter-chain exchange values is shown in Fig.6.

It should be mentioned that the multiplicative logarithmic factor in  $\chi'$ , eq.(51), does lead to a weak “spiral” instability at zero frequency – i.e. in this approach one finds a bound state with negative energy at some ordering momentum (measured from  $\pi$ ) [41]. This instability, however, is very weak. The corresponding ordering momentum is extremely small,  $k_{x,0} \sim 10^{-10}$  [41], translating into similarly tiny “instability energy”  $\sim Jk_{x,0}$ . Moreover, this classical instability is overshadowed by a stronger quantum (of collinear type) ones, of the order  $(J')^4/J^3$  [32]. Since our approximation is concerned with the features of the dynamical structure factor at energies of order  $J'$  and higher, we are allowed to disregard these weak instabilities.

*Anti-bound states* are analyzed similarly. In this case,  $\omega_t(\mathbf{k}) = \omega_{2,u}(k_x) + \delta_t(\mathbf{k})$  is above the 2-spinon continuum where  $\chi' < 0$ , see (49). Since  $\chi'(\omega)$  continuously decreases in magnitude to zero but retains the same (negative) sign as  $\omega$  in increased from  $\omega_{2,u}$  to  $\infty$ , the condition for the existence of an anti-bound state is simply  $1 + J'(\mathbf{k})\chi'(k_x, \omega_{2,u}) < 0$ . The anti-bound state therefore merges into the two-spinon continuum when  $1 + J'_{\text{crit}}(\mathbf{k})\chi'(k_x, \omega_{2,u}) = 0$ . As  $J'(\mathbf{k})$  is increased above this threshold, one can show that, because  $S(\mathbf{k}, \omega) \sim \text{Const} \sqrt{\omega_{2,u} - \omega}$  for  $\omega \lesssim \omega_{2,u}$  [42], the anti-bound state energy scales as  $\delta_t(\mathbf{k}) \propto (J'(\mathbf{k}) - J'_{\text{crit}}(\mathbf{k}))^2$  while its spectral weight scales as  $\sqrt{\delta_t}$ , similarly to the bound state situation discussed above. Unlike the bound state, the anti-bound one is not a completely sharp excitation. This is because it takes place in the region of 4-spinon excitations, which extend from  $\omega_{2,l}(k_x)$  up to  $\omega_{4,u}(k_x) = \pi J \sqrt{2(1 + |\cos[k_x/2]|)}$ , [40]. Hence,  $\chi'' \neq 0$  and the triplon lineshape is in fact Lorentian, see (48). However, the 4-spinon spectral weight is very small in the region between  $\omega_{2,u}$  and  $\omega_{4,u}$  boundaries [40], and we find that anti-bound states remain well defined, with the height-to-width ratio well above 1.

Being a collective excitation above the two-particle continuum, the anti-bound triplon here is very similar to the familiar zero-sound mode in a Fermi-liquid, e.g.  $^3\text{He}$ . The analogy is made much more precise by focusing on the region near  $\Gamma$  point in the Brillouin zone, where the 2-spinon continuum collapses onto a line:  $\omega_{2,u} - \omega_{2,l} \sim k_x^3$  as  $k_x \rightarrow 0$ . In this region  $\chi'(k_x, \omega) = |k_x|/(2(v_s|k_x| - \omega))$ , where  $v_s = \pi J/2$  is spinon velocity. The dispersion is found immediately (see Fig.2b):

$$\omega_t(\mathbf{k}) = v_s |k_x| \left( 1 + \frac{J'(\mathbf{k})}{2v_s} \right) \text{ for } J'(\mathbf{k}) > 0. \quad (52)$$

We see that the anti-bound triplon is just an “acoustic plasmon” of the spinon gas with short-range interactions.

As anti-bound states away from the  $\Gamma$  point require strong  $J'$  for their existence, we would like to suggest that somewhat more two-dimensional spatially anisotropic triangular antiferromagnet  $\text{Cs}_2\text{CuBr}_4$  [50] seems to be a promising candidate for the corresponding inelastic neutron scattering study.

---

[1] Haldane, F. D. M. ‘Luttinger liquid theory’ of one- dimensional quantum fluids. I. Properties of the Luttinger model and their extension to the general 1D interacting spinless Fermi gas. *J. Phys. C* **14**, 2585-2609 (1981).

- [2] Lieb, E. H. & Wu, F. Y. Absence of Mott Transition in an Exact Solution of the Short-Range, One-Band Model in One Dimension. *Phys. Rev. Lett.* **20**, 1445-1448 (1968).
- [3] Faddeev, L. D. & Takhtajan, L. A. What is the spin of a spin wave? *Phys. Lett. A* **85**, 375-377 (1981).
- [4] Haldane, F. D. M. "Spinon gas" description of the  $S=1/2$  Heisenberg chain with inverse-square exchange: Exact spectrum and thermodynamics. *Phys. Rev. Lett.* **66**, 1529-1532 (1991).
- [5] Bloch, F. Zur Theorie des Ferromagnetismus. *Z. Phys.* **61**, 206-219 (1930).
- [6] Anderson, P. W. An Approximate Quantum Theory of the Antiferromagnetic Ground State. *Phys. Rev.* **86**, 694-701 (1952).
- [7] Kubo, R. The Spin-Wave Theory of Antiferromagnetics. *Phys. Rev.* **87**, 568-580 (1952).
- [8] Anderson, P. W. Resonating valence bonds: A new kind of insulator? *Mater. Res. Bull.* **8**, 153-160 (1973).
- [9] Kivelson, S. A., Rokhsar, D. S. & Sethna, J. P. Topology of the resonating valence-bond state: Solitons and high-  $T_c$  superconductivity. *Phys. Rev. B* **35**, 8865-8868 (1987).
- [10] Kotliar, G. & Ruckenstein, A. E. New Functional Integral Approach to Strongly Correlated Fermi Systems: The Gutzwiller Approximation as a Saddle Point. *Phys. Rev. Lett.* **57**, 1362-1365 (1986).
- [11] Zou Z. & Anderson, P. W. Neutral fermion, charge-e boson excitations in the resonating-valence-bond state and superconductivity in  $\text{La}_2\text{CuO}_4$ -based compounds. *Phys. Rev. B* **37**, 627-630 (1988).
- [12] Lee, P. A., Nagaosa, N. & Wen, X.-G. Doping a Mott insulator: Physics of high-temperature superconductivity. *Rev. Mod. Phys.* **78**, 17-85 (2006).
- [13] Senthil, T., Vishwanath, A., Balents, L., Sachdev, S. & Fisher, M.P.A. Deconfined Quantum Critical Points. *Science* **303**, 1490-1494 (2004).
- [14] Kashima, T. & Imada, M. Magnetic and Metal-Insulator Transitions through Bandwidth Control in Two-Dimensional Hubbard Models with Nearest and Next-Nearest Neighbor Transfers. *J. Phys. Soc. Jpn.* **70**, 3052-3067 (2001).
- [15] Morita, H., Watanabe, S. & Imada, M. Nonmagnetic Insulating States near the Mott Transitions on Lattices with Geometrical Frustration and Implications for  $\kappa$ -( $\text{ET}$ ) $_2\text{Cu}_2(\text{CN})$ . *J. Phys. Soc. Jpn.* **71**, 2109-2112 (2002).
- [16] Coldea, R., Tennant, D.A., Tsvetlik, A.M. & Tylczynski, Z. Experimental Realization of a 2D Fractional Quantum Spin Liquid. *Phys. Rev. Lett.* **86**, 1335-1338 (2001).
- [17] Coldea, R., Tennant, D. A. & Tylczynski, Z. Extended scattering continua characteristic of spin fractionalization in the two-dimensional frustrated quantum magnet  $\text{Cs}_2\text{CuCl}_4$  observed by neutron scattering. *Phys. Rev. B* **68**, 134424 (2003).
- [18] Shimizu, Y., Miyagawa, K., Kanoda, K., Maesato, M. & Saito, G. Spin Liquid State in an Organic Mott Insulator with a Triangular Lattice. *Phys. Rev. Lett.* **91**, 107001 (2003).
- [19] Helton, J.S. *et al.*, Spin Dynamics of the Spin-1/2 Kagome Lattice Antiferromagnet  $\text{ZnCu}_3(\text{OH})_6\text{Cl}_2$ . *Phys. Rev. Lett.* **98**, 107204 (2007).
- [20] Ofer, O. *et al.*, Ground state and excitation properties of the quantum kagomé system  $\text{ZnCu}_3(\text{OH})_6\text{Cl}_2$  investigated by local probes, cond-mat/0610540.
- [21] Masutomi, R., Karaki, Y. & Ishimoto, H. Gapless Spin Liquid Behavior in Two-Dimensional Solid  $^3\text{He}$ . *Phys. Rev. Lett.* **92**, 025301 (2004).
- [22] Coldea, R. *et al.* Direct Measurement of the Spin Hamiltonian and Observation of Condensation of Magnons in the 2D Frustrated Quantum Magnet  $\text{Cs}_2\text{CuCl}_4$ . *Phys. Rev. Lett.* **88**, 137203 (2002).
- [23] Yi Zhou, Xiao-Gang Wen, Quantum Orders and Spin Liquids in  $\text{Cs}_2\text{CuCl}_4$ , arXiv:cond-mat/0210662v3 (2002).
- [24] Aicea, J., Motrunich, O. I. & Fisher, M. P. A. Algebraic Vortex Liquid in Spin-1/2 Triangular Antiferromagnets: Scenario for  $\text{Cs}_2\text{CuCl}_4$ . *Phys. Rev. Lett.* **95**, 247203 (2005).
- [25] Isakov, S. V., Senthil, T. & Kim, Y. B. Ordering in  $\text{Cs}_2\text{CuCl}_4$ : Possibility of a proximate spin liquid. *Phys. Rev. B* **72**, 174417 (2005).
- [26] Veillette, M. Y., James, A. J. A. & Essler, F. H. L. Spin dynamics of the quasi-two-dimensional spin-1/2 quantum magnet  $\text{Cs}_2\text{CuCl}_4$ . *Phys. Rev. B* **72**, 134429 (2005).
- [27] Dalidovich, D., Sknepnek, R., Berlinsky, A. J., Zhang, J. & Kallin, C. Spin structure factor of the frustrated quantum magnet  $\text{Cs}_2\text{CuCl}_4$ . *Phys. Rev. B* **73**, 184403 (2006).
- [28] Zheng, W., Fjærestad, J. O., Singh, R. R. P., McKenzie, R. H. & Coldea, R. Anomalous Excitation Spectra of Frustrated Quantum Antiferromagnets. *Phys. Rev. Lett.* **96**, 057201 (2006).
- [29] Fjærestad, J. O., Zheng, W., Singh, R. R. P., McKenzie, R. H. & Coldea, R., Excitations spectra and ground state properties of layered spin-1/2 frustrated antiferromagnets  $\text{Cs}_2\text{CuCl}_4$  and  $\text{Cs}_2\text{CuBr}_4$ . cond-mat/0701014.
- [30] J. M. Wheatley, T. C. Hsu, and P. W. Anderson, Interlayer pair hopping: Superconductivity from the resonating- valence-bond state, *Phys. Rev. B* **37**, 5897 - 5900 (1988).
- [31] Chakravarty, S., Sudbø, A., Anderson, P. W. & Strong, S. Interlayer Tunneling and Gap Anisotropy in High- Temperature Superconductors. *Science* **261**, 337-340 (1993).
- [32] Starykh, O. A. & Balents, L. Ordering in Spatially Anisotropic Triangular Antiferromagnets, *Phys. Rev. Lett.* **98**, 077205 (2007).
- [33] W. Zheng, R.H. McKenzie, and R.R.P. Singh, Phase diagram for a class of spin-1/2 Heisenberg models interpolating between the square-lattice, the triangular-lattice, and the linear-chain limits, *Phys. Rev. B* **59**, 14367 - 14375 (1999).
- [34] M. Q. Weng, D. N. Sheng, Z. Y. Weng, Robert J. Bursill, Spin Liquid Phase in Anisotropic Triangular Lattice Heisenberg Model: Exact diagonalization and density-matrix renormalization group calculations, *Phys. Rev. B* **74**, 012407 (2006).
- [35] Bethe, H. Zur Theorie der Metalle. I. Eigenwerte und Eigenfunktionen der linearen Atomkette. *Z. Phys.* **71**, 205-226 (1931).
- [36] Hulthén, L. Über das Austauschproblem eines Kristalles. *Arkiv Mat. Astron. Fysik* **26A**, No.11, 1-106 (1938).
- [37] J. des Cloizeaux and J.J. Pearson, Spin-Wave Spectrum of the Antiferromagnetic Linear Chain, *Phys. Rev.* **128**, 2131

- (1962).
- [38] Müller, G., Thomas, H., Beck, H. & Bonner, J. C. Quantum spin dynamics of the antiferromagnetic linear chain in zero and nonzero magnetic field. *Phys. Rev. B* **24**, 1429-1467 (1981).
  - [39] Bougourzi, A.H., Couture, M. & Kacir, M. Exact two- spinon dynamical correlation function of the one-dimensional Heisenberg model. *Phys. Rev. B* **54**, R12669-R12672 (1996).
  - [40] J.-S. Caux and R. Hagemans, The 4-spinon dynamical structure factor of the Heisenberg chain, *J. Stat. Mech.* (2006) P12013.
  - [41] Bocquet, M., Essler, F. H. L., Tsvetlik, A. M. & Gogolin, A. O. Finite-temperature dynamical magnetic susceptibility of quasi-one-dimensional frustrated spin-1/2 Heisenberg antiferromagnets. *Phys. Rev. B* **64**, 094425 (2001).
  - [42] Karbach, M., Müller, G., Bougourzi, A.H., Fledderjohann, A. & Mütter, K.-H. Two-spinon dynamic structure factor of the one-dimensional  $s=1/2$  Heisenberg antiferromagnet. *Phys. Rev. B* **55**, 12510-12517 (1997).
  - [43] Kitanine, N., Maillet, J. M. & Terras, V. Form factors of the XXZ Heisenberg spin-1/2 finite chain. *Nucl.Phys. B* **554**, 647 (1999).
  - [44] Biegel, D., Karbach, M. & Müller, G. Transition rates via Bethe ansatz for the spin-1/2 planar XXZ antiferromagnet. *J. Phys. A: Math. Gen.* **36** 5361 (2003).
  - [45] Caux, J. -S., Hagemans, R. & Maillet, J. M. Computation of dynamical correlation functions of Heisenberg chains: the gapless anisotropic regime. *J. Stat. Mech.* P09003 (2005).
  - [46] A.A. Abrikosov, L. P. Gorkov and I. E. Dzyaloshinski, *Methods of Quantum Field Theory in Statistical Physics*, (Dover, New York, 1975).
  - [47] Scalapino, D. J., Imry, Y. & Pincus, P. Generalized Ginzburg-Landau theory of pseudo-one-dimensional systems. *Phys. Rev. B* **11**, 2042-2048 (1975).
  - [48] Schulz, H. J. Dynamics of Coupled Quantum Spin Chains. *Phys. Rev. Lett.* **77**, 2790-2793 (1996).
  - [49] Starykh, O. A. & Balents, L. Dimerized Phase and Transitions in a Spatially Anisotropic Square Lattice Antiferromagnet. *Phys. Rev. Lett.* **93**, 127202 (2004).
  - [50] T. Ono *et al.*, Magnetization plateaux of the  $S = 1/2$  two-dimensional frustrated antiferromagnet  $\text{Cs}_2\text{CuBr}_4$ , *J.Phys.: Condens. Matter* **16**, S773-S778 (2004).

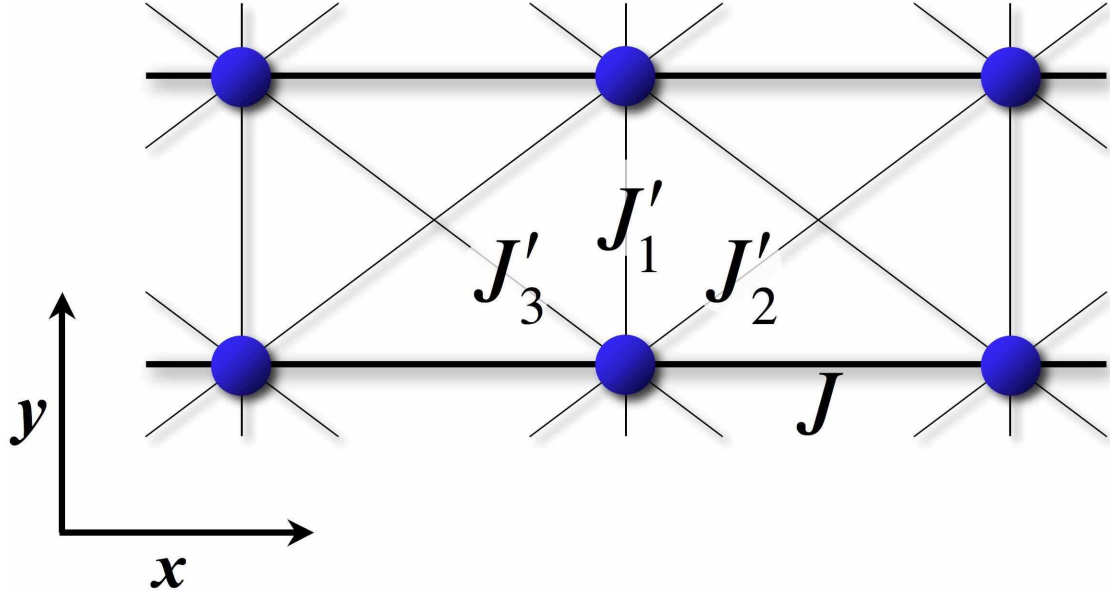


FIG. 1: Lattice structure and coupling constants  $J_1'$ ,  $J_2'$ ,  $J_3'$  and  $J$ . Dots and lines denote sites and bonds, respectively.

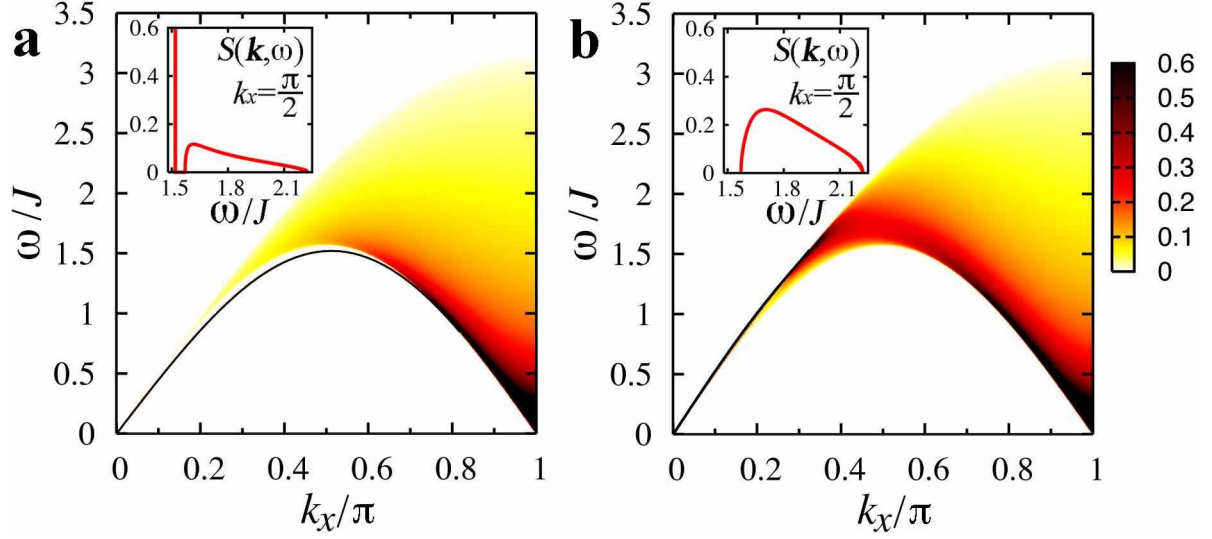


FIG. 2: Density plot of dynamical Structure factor  $S(\mathbf{k}, \omega)$  for  $J_2' = J_3' = J_1'/2 = 0.24J$  at (a)  $k_y = \pi$  and (b)  $k_y = 0$ . The insets show the plots at  $k_x = \pi/2$ .

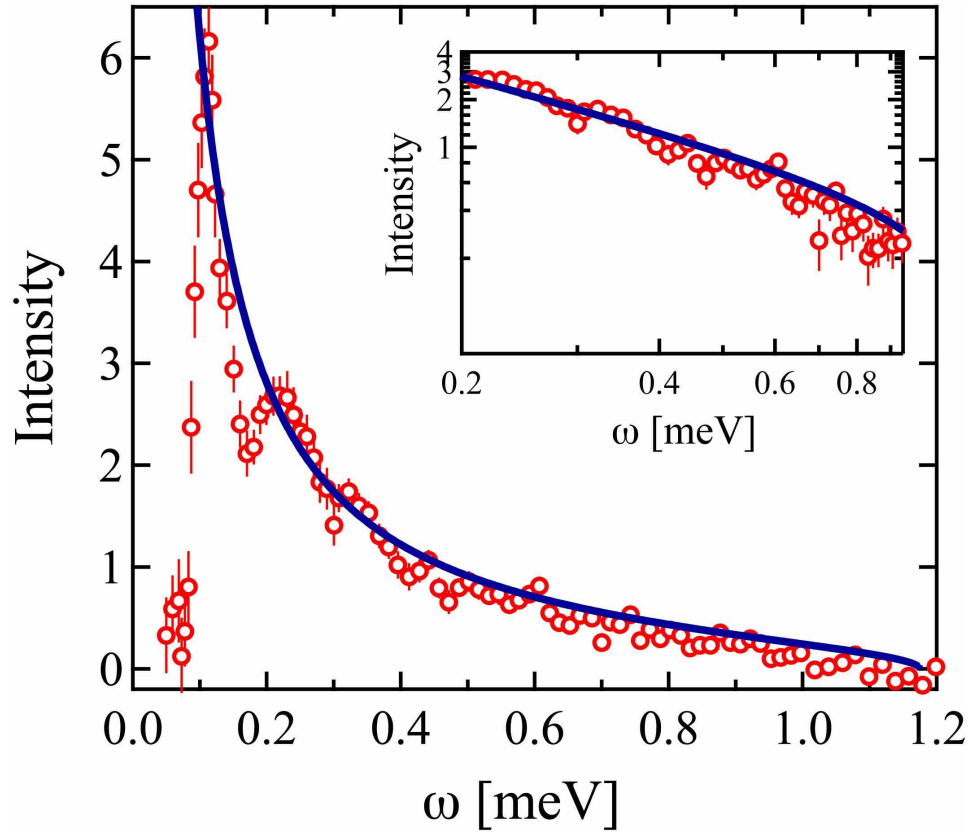


FIG. 3: Comparison with the experimental result for dynamical structure factor  $S(\mathbf{k}, \omega)$  at  $k'_x = \pi$ . Solid line denotes the two-spinon structure factor  $S_{1D}(\pi, \omega)$  of a single chain with exchange  $J = 0.374$  meV[17]. The symbols are the experimental data obtained by the inelastic neutron scattering experiment on  $\text{Cs}_2\text{CuCl}_4$ , taken from the G scan of Fig. 5 in Ref. [17]. The inset shows the log-log plot. The theoretical result is fitted to the experimental data by adjusting the height with a single multiplication factor. The experimental data in this and the following figures are excerpted with permission from Ref. [17]. Copyright (2003) by the American Physical Society.

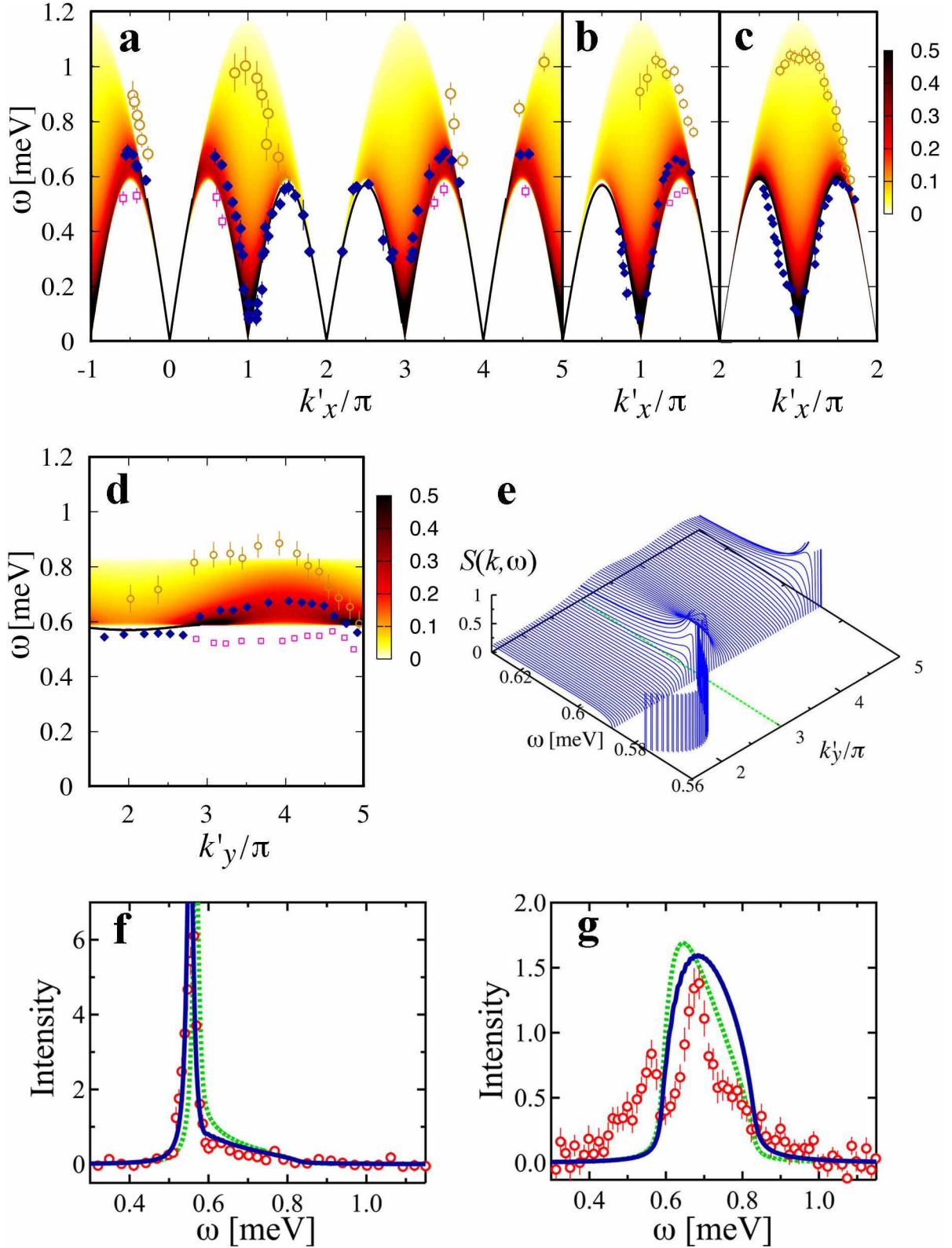


FIG. 4: **a.-d.** Comparison with experimental results for dispersion relations at (a)  $k'_y=0$ , (b)  $k'_y=2\pi$ , (c)  $k'_y=3\pi$  and (d)  $k'_x=-\pi/2$ . Density plots are the present results of dynamical structure factor  $S(\mathbf{k}, \omega)$  for  $J'_1 = J'_2 = 0.34J$ ,  $J'_3 = 0$  and  $J=0.374$  meV. Solid and open symbols denote the main peak, and the upper and lower edges of the spectrum observed by the neutron scattering experiment on  $\text{Cs}_2\text{CuCl}_4$ , respectively, taken from Ref. [17]. Graphs (a)-(d) correspond to (1), (3), (4) and (2) of Fig. 3 in Ref. [17], respectively. **e.**  $S(\mathbf{k}, \omega)$  at  $k'_x = -\pi/2$  near the lower edge of continuum obtained by the present approach. The sign of  $J'(\mathbf{k})$  changes at  $k'_y = 3\pi$ . **f.-g.** Comparison with experimental data for the line shape of  $S(\mathbf{k}, \omega)$  at (f)  $\mathbf{k}' = (-\pi/2, 2\pi)$  and (g)  $\mathbf{k}' = (-\pi/2, 4\pi)$ . Dotted lines are present results within the 2-spinon subspace multiplied by the normalization factor obtained by fitting the G scan in Fig.3. Solid lines are RPA result which accounts for the 4-spinon states as obtained in a chain of length  $L_x = 288$ , see main text for the details. The numerical data in f and g are broadened by energy resolution  $\Delta E = 0.019$  meV of the spectrometer [17] including the isotropic magnetic form factor of  $\text{Cu}^{2+}$  ions. Symbols are experimental data for (f) E scan and (g) F scan of Fig. 5 in Ref. [17].

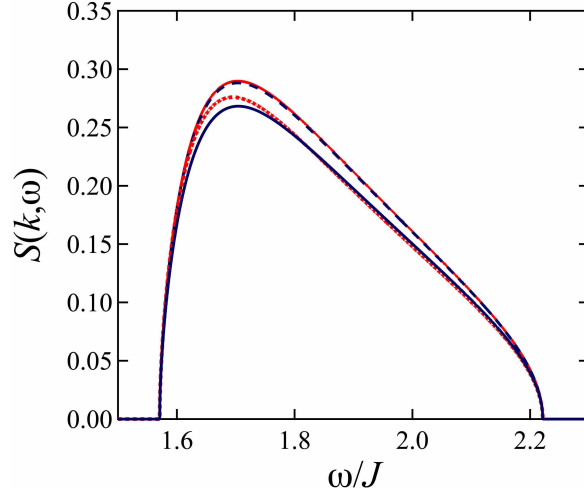


FIG. 5: Comparison of  $S(\mathbf{k}, \omega)$  at  $\mathbf{k}' = (-\pi/2, 4\pi)$  between the present approximation (17) and (30) (blue solid line), that without the correction to the ground state (blue dashed line), RPA as derived in (4), (48) and (49) (red line), and the standard RPA (50) (dotted red line).

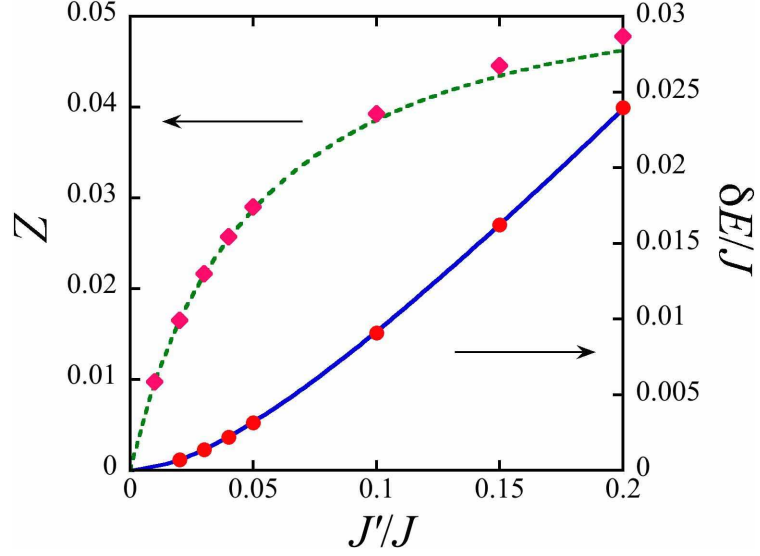


FIG. 6: (Left  $y$ -axis) Transition rate to the bound state ( $Z$ ). Pink diamonds are obtained by the present approach, and the green dotted line is the analytical result in Eq.(44). The small deviation in the large  $J'/J$  regime is due to the correction to the ground state which is not included in Eq.(44). (Right  $y$ -axis) Gap between the bound state and the lower edge of continuum ( $\delta E$ ). Red circles are obtained by the present approach, and the blue solid line denotes the RPA result. The data shown here are calculated at  $\mathbf{k} = (\pi/4, \pi)$  on a spatially anisotropic triangular lattice with  $J'_1 = J'_2 (\equiv J')$  and  $J'_3 = 0$ .